Atmospheric
Chemistry
and Physics
Discussions

Open Access

Climatology of free tropospheric humidity: extension into the SEVIRI era, evaluation and exemplary analysis

M. Schröder[1], R. Roca[2], L. Picon[3], A. Kniffka[1], and H. Brogniez[4]

[1]Satellite-Based Climate Monitoring, Deutscher Wetterdienst, Offenbach, Germany
[2]OMP/LEGOS/CNRS, Toulouse, France
[3]Sorbonne Universités, UPMC Univ. Paris 06; CNRS/INSU; ENS; Ecole Polytechnique; LMD-IPSL, UMR 8539, Paris, France
[4]Université Versailles St-Quentin; Sorbonne Universités, UPMC Univ. Paris 06; CNRS/INSU; LATMOS-IPSL, Guyancourt, France

Correspondence to: M. Schröder (marc.schroder@dwd.de)

Discussion Paper | Discussion Paper | Discussion Paper | Discussion Paper

ACPD

14, 9603–9646, 2014

Climatology of free tropospheric humidity

M. Schröder et al.

Title Page

Abstract	Introduction
Conclusions	References
Tables	Figures

◄◄ | ►►

◄ | ►

Back | Close

Full Screen / Esc

Printer-friendly Version

Interactive Discussion

Abstract

A new free tropospheric humidity (FTH) data record is presented. It is based on observations of Meteosat-2–5 and Meteosat-7 Meteosat Visible and Infrared Imager (MVIRI) and Meteosat-8 and -9 Spinning Enhanced Visible and Infrared Imager (SEVIRI) at

5 the water absorption band at 6.3 μm. With the extension to SEVIRI observations the data record now covers the period 1983–2009 with a spatial and temporal resolution of 0.625° and 3 h, respectively. The data record is referenced under digital object identifier (doi): 10.5676/EUM_SAF_CM/FTH_METEOSAT/V001 and is freely available from http://www.cmsaf.eu/wui.

10 The relation between the observed brightness temperature (BT) and FTH is well established: the observed BT is proportional to the logarithm of the mean relative humidity (RH). Under the given assumptions, constant lapse rate and random strong line theory, it means that the observed BT is mainly a function of RH alone and not of temperature and specific humidity separately. Here, existing retrievals have been refined

15 mainly through the consideration of relative humidity Jacobians in the training process of the statistical retrieval. The temporal coverage has been extended into the SEVIRI era, the homogenisation of the BT record has been improved and the full archive has been reprocessed using updated regression coefficients.

The FTH product is compared against FTH computed on the basis of the Analysed

20 RadioSoundings Archive (ARSA) observations. An average relative bias and root mean square difference (RMSD) of −3.2 and 16.8 %, respectively, are observed. The RMSD confirms the expectation from an analysis of the total uncertainty of the FTH product. The decadal stability is 0.5 ± 0.45 % per decade.

As exemplary applications the inter-annual standard deviation, differences on

25 decadal scales and the linear trend in the FTH data record and the frequency of occurrence of FTH < 10 % (FTHp10) are analysed per season. Maxima in inter-annual standard deviations as well as maxima in absolute differences occur in gradient areas between dry and wet regions and areas with minima in FTH and maxima in FTHp10. An

Climatology of free tropospheric humidity

M. Schröder et al.

Title Page

Abstract	Introduction
Conclusions	References
Tables	Figures

|◀ | ▶|

◀ | ▶

Back | Close

Full Screen / Esc

Printer-friendly Version

Interactive Discussion

analysis of the linear trends and associated uncertainty estimates has been attempted to identify possible problems with the data record. Positive trends in FTHp10 coincide with gradient areas and regions of minimum FTH, maximum FTHp10 as well as with negative differences between decadal FTHp10 averages of the 1990s and 2000s. However, they are accompanied by maximum standard deviation and are therefore hardly significant which is also valid for FTH trend estimates. These activities plus inter-comparisons to other humidity data records are part of the Global Energy and Water Exchanges Project (GEWEX) water vapor assessment (G-VAP) and will be extended to other FTH data records in the near future.

1 Introduction

Water vapour plays a central role in the Earth's energy and water cycles and is the most effective greenhouse gas, making it a key variable for climate analysis. Water vapour has an amplifying role in a warming environment through a strong positive climate feedback loop as evident in climate predictions, and this water vapour feedback loop is dominated by water vapour in the tropical free troposphere (Held and Soden, 2000). The importance of humidity in the free troposphere originates from the non-linear interaction between humidity and long-wave radiation. In order to realistically assess this impact the full probability distribution needs to be considered. It can however be concluded that outgoing longwave radiation (OLR) is much more sensitive to perturbations at the dry end than at the moist part of the distribution (Spencer and Braswell, 1997; Roca et al., 2012a). Sherwood et al. (2010a) recently reviewed the processes that determine the humidity distribution in the intertropical region. They emphasize the strong connection between the large scale dynamics and water vapour and the roles of eddies (mesoscale convection, circulation transients) in establishing these links pointing out to a broad range of scale implied in the humidity distribution. They further indicate that there is a need to better constrain the available theory. Satellites that observe the humidity of the free troposphere, and particularly, geostationary platforms are very well

suited to contribute to this constraint by providing observations at kilometres and hours scale resolution over a 30 years long period.

In general infrared imagers and infrared sounders with channels centred at the water vapour absorption band around 6.3 µm as well as microwave sounders with channels centred at 183.31 GHz allow for sounding of the free troposphere. The commonly applied relationship between observed BT and FTH was developed by Soden and Bretherton (1993) for infrared observations and relies on the assumptions of random strong line theory and constant lapse rate. The proportionality is relative to a vertical average of the relative humidity in the free troposphere. The regression coefficients depend on the averaging kernel and the performance of the regression can be improved with the consideration of the so-called scaled reference pressure. Based on the work of Soden and Bretherton (1993, 1996), Roca et al. (2003) determined the regression coefficients statistically and used reanalyses to determine the scaled reference pressure while Schmetz et al. (1995) uses reanalyses to determine regression coefficients on pixel basis. Both retrievals were originally designed for MVIRI observations. Buehler and John (2005) adapted the method described in Soden and Bretherton (1996) to intercalibrated Advanced Microwave Sounding Unit-B (AMSU-B) observations (John et al., 2013). The AMSU-B based FTH data record is affected by orbital drift and contains valid observations under all sky conditions except in presence of intense scattering such as during precipitation events. Recently, the method described in Soden and Bretherton (1996) has also been adjusted to three of the six channels of the Sondeur Atmosphérique du Profil d'Humidité Intertropicale par Radiometrie (SAPHIR) onboard the Megha-Tropiques satellite (Brogniez et al., 2014) which was launched in October 2011. Shi and Bates (2011) spent significant effort on recalibrating and intercalibrating the water vapour observations at 6.7 µm of the High-resolution Infrared Radiation Sounder (HIRS). A subsequent application of the Soden and Bretherton (1996) method yields a FTH record of more than 30 years length (Shi et al., 2013). The time series is affected by orbital drift and, as for the MVIRI observations, FTH is retrieved under clear sky and low level cloud conditions. Jackson and Bates (2001) assessed free

tropospheric humidity algorithms applicable to HIRS observations at 6.7 µm. Among other things they concluded that the averaging kernel has a significant effect on the FTH retrieval and that the consideration of scaled reference pressure (see Soden and Bretherton, 1996) in the retrieval improves results in the tropics.

Brogniez et al. (2009) assessed the quality of the Meteosat based FTH record for the period 1984–2005 by comparison against a previous ARSA version. They found a bias of −1.2 %RH with a standard deviation of 1.7 %RH. The value of the FTH product has been demonstrated, e.g., in Brogniez et al. (2005) who compared the FTH product against 14 climate models in the framework of the Atmospheric Model Intercomparison Project (AMIP) phase 2. Buehler et al. (2008) estimated the theoretical uncertainty of the AMSU-B based FTH retrieval scheme: 2 %RH and 7 %RH in bias for low and high values of FTH, respectively. John et al. (2011) further found a systematic clear sky bias of 9 %RH by sampling the all sky AMSU-B product with the HIRS clear sky mask and comparing the clear sky and all sky AMSU-B UTH products. An exemplary application of the AMSU-B UTH data record is given in Moradi et al. (2010). They demonstrate a coincidence of the difference between AMSU-B data and the Integrated Global Radiosonde Archive (IGRA, Durre et al., 2006) with the spatial distribution of radiosonde types. The HIRS based FTH data record has been evaluated in radiance space (see Shi and Bates, 2011), and the correlation of the BT to various climate indices has been analysed, among others, showing the potentially valuable contribution of this data record to analyse global teleconnections.

Most of our knowledge about the impact of climate change on FTH arises from theoretical or global average considerations (Pierrehumbert et al., 2007; Sherwood et al., 2010b; Shi and Bates, 2011; Roca et al., 2012a and references therein). At a global scale the assumption of constant relative humidity is supported by the work of, e.g., Soden and Held (2000) and Soden et al. (2002). However, it can be expected that water vapour pressure is typically below equilibrium in most of the atmosphere. This is particularly true for the dry regions in the free troposphere where perturbations would have a large impact on OLR. Efforts passing through this information to the regional

scale are few and are considered as difficult tasks. At the zonal mean scale though, a common pattern emerges for a doubling of CO_2: dry region shifts pole wards (Sherwood et al., 2010a), dry minimum gets drier (Hurley and Galewsky, 2010) and the dry region width increases. Such climate change impacts on FTHp10 were observed from the IPSL (Institut Pierre Simon Laplace) climate model based on the analysis of the FTH distribution under a climate change scenario (Roca et al., 2012a). At a more regional scale, it is very difficult to assess whether any of these large scale features is reproduced and if not what is the expected pattern modification. Furthermore, it is important to recall that such modifications are contrasted for doubling of CO_2 and it is not obvious to interpret how these model-derived perspectives have been at play over the last 25 years. In any case, a much smaller response is anticipated than the response after CO_2 is doubled as in the scenario used in Roca et al. (2012a). As a consequence, it is important to keep in mind that an analysis of currently available FTH data records in this context is preliminary.

Activities related to the generation of FTH data sets from Meteosat, AMSU-B and HIRS were part of a pilot project within the World Meteorological Organisation (WMO) Sustained, Coordinated Processing of Environmental Satellite Data for Climate Monitoring (SCOPE-CM). The aim of SCOPE-CM is to establish a network of facilities ensuring continuous and sustained provision of high-quality satellite products related to the Essential Climate Variables (ECV), on a global scale, responding to the requirements of the Global Climate Observing system (GCOS). Recently, SCOPE-CM initiated its second phase that aims at advancing the maturity of Climate Data Records constructed from satellite data. Under the SCOPE-CM umbrella the Meteosat, AMSU-B and HIRS data records will be aligned in format, metadata and documentation to the maximum extent possible to meet the aim of SCOPE-CM's second phase. Also, within a SCOPE-CM project observations from all available geostationary imagers will be recalibrated and intercalibrated. The impact of this Fundamental Climate Data Record (FCDR) on the Meteosat based FTH product will be evaluated within this activity as well.

Climatology of free tropospheric humidity

M. Schröder et al.

Printer-friendly Version

Interactive Discussion

The GEWEX Data and Assessments Panel (GDAP) has initiated a Water Vapor Assessment, the G-VAP. One element of G-VAP is the intercomparison of available long-term FTH data records and the analysis and comparison of temporal changes in these data sets. The application part of the work presented here supports the latter G-VAP activity by setting-up the technical framework and starting the analysis with the Meteosat based FTH data set.

The input data and the homogenisation of Meteosat observations are introduced in Sects. 2 and 3, respectively. This is followed by a description of the retrieval scheme that also provides an overview of the data record's technical specifications and exemplary figures on the appearance of the FTH data record. After a discussion of the uncertainty budget evaluation results are shown in Sect. 6. The applications in Sect. 7 start with an analysis of the variability and differences on decadal scales, followed by an analysis of the linear trend. Finally, we provide conclusions.

2 Input data

This section briefly describes the instruments and input data sets that have been used to retrieve FTH. These data sets are described in the following order: (1) radiance data sets and (2) reanalysis. Finally, the radiative transfer model RTTOV, which was applied during retrieval development and evaluation, is briefly introduced.

The Meteosat Visible and Infrared Imager (MVIRI) is a three channel imaging radiometer flown consecutively on Meteosat-2 to Meteosat-7 from the first generation of Meteosat satellites. It observes the Earth from a geostationary orbit at 0° latitude orbit every 30 min between 1982 and 2006. The spatial sampling distance of the observations is approximately 5 km at nadir and increases with distance from the sub-satellite point.

The Spinning Enhanced Visible and Infrared Imager (SEVIRI) carries out observations at 12 channels covering the visible and thermal infrared spectral wavelength range. SEVIRI is on board Meteosat-8 and 9, which are geostationary satellites

Climatology of free tropospheric humidity

M. Schröder et al.

positioned at 0° latitude while in operational mode. SEVIRI full disc observations are repeated every 15 min between 2004 and present. The spatial sampling distance is 3 km, again increasing with distance from the sub-satellite point.

The elaboration of the Meteosat clear sky radiance (CSR) archive is described at length in Brogniez et al. (2006, 2009) and partly recalled in Sect. 3. The 6.3 µm BTs, as observed by Meteosat-2 to 5 as well as Meteosat-7, together with cloud cover and cloud top pressure are taken from the International Satellite cloud Climatology Project (ISCCP, Rossow and Schiffer, 1999, DX level). In addition to the clear-sky pixels, low-level clouds with a cloud-top pressure larger than 680 hPa are kept, improving significantly the sampling. All observations are adapted to the Meteosat-5 spectral response function. The CSR archive from LMD, with Meteosat-5 as reference is utilised as input and covers the July 1983–June 2005 period. This CSR record has been extended using ISCCP-DX data for the period July 2005–June 2006. From July 2006 onwards SEVIRI observations in sensor resolution are sampled to mimic ISCCP-DX radiance data. Cloud information is taken from ISCCP-DX (July 1983–December 2009).

3   Homogenisation and extension to the SEVIRI era

Prior to the inversion to FTH, the CSR data record is adapted to the Meteosat-5 spectral response function. Scatterplots of simulated Meteosat-5 and Meteosat-8 as well as Meteosat-5 and Meteosat-9 exhibit excellent linear behaviour so that a linear equation with slope a and intercept b is used for adaptation (not shown). The coefficients for Meteosat-5/Meteosat-8 and for Meteosat-5/Meteosat-9 are $a = 1.0160$ and $b = -2.3498$ as well as $a = 1.0174$ and $b = -2.6033$, respectively.

Mainly due to satellite changes and changes in calibration the Meteosat time series is not fully homogeneous but exhibits breakpoints in BT time series. Such breakpoints can be eliminated using homogenisation approaches. The homogenisation applied here largely follows the work of Picon et al. (2003).

Title Page

Abstract | Introduction

Conclusions | References

Tables | Figures

◀ | ▶

◀ | ▶

Back | Close

Full Screen / Esc

Printer-friendly Version

Interactive Discussion

The basic approach is to utilise the ECMWF reanalyses ERA-Interim (Dee et al., 2011) data as input to RTTOV9.3 simulations of Meteosat-5 observations, to simulate Meteosat-5-like BT and apply linear regression to the observed BT for a month prior and after the breakpoint (adapted from Picon et al., 2003):

$$\text{BT}_{\text{corrected}} = \frac{a_{\text{before}}}{a_{\text{after}}}\text{BT}_{\text{original}} + b_{\text{before}} - b_{\text{after}}\frac{a_{\text{before}}}{a_{\text{after}}} = a'\text{BT}_{\text{original}} + b' \tag{1}$$

Output from the regression is used to modify the satellite observed BT such that bias and root mean square difference (RMSD) between observed and simulated BT are preserved. The underlying assumption is stability of ERA-Interim simulations over the two months.

In order to carry out the comparison the following criteria have been applied:

– Only data at 06:00 and 12:00 UTC have been considered.

– Simulations are performed in clear sky only. This is further constrained by considering the warmest 80 % in simulated radiances only.

– The subdomain covers ±45° N/S and ±45° E/W.

– After double application of the linear regression and substituting for simulated BT the homogenization coefficients a' and b' can be computed.

This approach is applied to homogenise the change in calibration in January 2001 as well as the Meteosat-7/8 and Meteosat-8/9 transitions using ERA-Interim data for the months December 2000 and January 2001, June and July 2006, and April and May 2007, respectively. The following parameters have been computed and applied:

– January 2001 onwards: $a' = 0.98908$ and $b' = 2.10135$.

– July 2006 onwards: $a' = 1.01510$ and $b' = 1.00681$.

– May 2007 onwards: $a' = 0.974119$ and $b' = 5.31705$.

Title Page

Abstract | Introduction

Conclusions | References

Tables | Figures

|◄ | ►|

◄ | ►

Back | Close

Full Screen / Esc

Printer-friendly Version

Interactive Discussion

After homogenization, the inter-calibration to HIRS (Breon et al., 2000) is applied to the CSR data. Then, the results are consistent with HIRS channel 12 observations on NOAA12 and the known bias of Meteosat-5 is removed.

Figure 1 shows the deseasonalised anomaly of the original and the updated BT. The change in difference in January 2001, July 2006 and May 2007 is 0.5 K, 4.5 K, and 0.8 K, respectively. Obviously the degree of homogeneity and stability has been largely improved.

A brief discussion of potential reasons for the breakpoints and results from other activities follows. Results from the Global Space-based Inter-Calibration System (GSICS) for May to December 2008 exhibit a difference in bias between Meteosat-8 and Meteosat-9 relative to Infrared Atmospheric Sounding Interferometer (IASI) of slightly less than 0.5 K. The magnitude of the bias and the observing period are different but confirms the bias between Meteosat-8 and Meteosat-9 in the early Meteosat-9 phase. Note that this bias is significantly smaller in 2009 and onwards.

As far as the first generation is concerned, in May 2000 the vicarious calibration has been replaced with the calibration using the onboard black body, and an updated version has been implemented in January 2001 (http://www.eumetsat.int/website/wcm/idc/idcplg?IdcService=GET_FILE&dDocName=PDF_TEN_BLACKBODY-CALIBRATION&RevisionSelectionMethod=LatestReleased&Rendition=Web). In parallel the eclipse of the years 2000 and 2001 affected the overall performance (Köpken, 2001). Finally a series of gain changes, in particular also on 09 January 2001 (http://www.eumetsat.int/website/wcm/idc/idcplg?IdcService=GET_FILE&dDocName=PDF_REP_GAINS_HIST_MET7&RevisionSelectionMethod=LatestReleased&Rendition=Web) has been applied.

Climatology of free tropospheric humidity

M. Schröder et al.

Title Page

Abstract | Introduction

Conclusions | References

Tables | Figures

◄ | ►

◄ | ►

Back | Close

Full Screen / Esc

Printer-friendly Version

Interactive Discussion

4 Retrieval scheme

Assuming random strong line theory and constant lapse rate Soden and Bretherton (1993) showed that the observed BT is proportional to the logarithm of the mean relative humidity (RH) over a deep layer of the troposphere. Under the given assumptions it means that the observed BT is mainly a function of RH alone and not of temperature and specific humidity separately. The Free Tropospheric Humidity (FTH) is determined from the following equation, analytically determined by Soden and Bretherton (1996):

$$\ln\left(\frac{\langle RH\rangle p_0}{\cos\theta}\right) = a \times BT_{6.3\,\mu m} + b. \tag{2}$$

This equation links the clear sky BT of a 6.3 μm channel to the mean relative humidity (RH, in % defined with respect to water only) of a broad layer of the troposphere. Equation (2) also makes use of a correction of the satellite viewing angle θ and a scaling parameter p_0, which is defined as the ratio of the pressure at a temperature of 240 K to 300 hPa. p_0 represents the deviation from a standard tropical profile where the 240 K isotherm is located at 300 hPa (see Soden and Bretherton, 1993). ERA-Interim and ERA-40 (Uppala et al., 2005) data are used to determine the thermal parameter p_0. Both reanalysis data sets are available on sigma hybrid model levels (ML) and standard pressure levels (PL). In Roca et al. (2009) it was demonstrated that the vertical resolution does not affect FTH quality significantly as long as a certain minimum number of pressure levels is present. Thus, ERA-Interim (since January 2006) and ERA40 (until December 2005) ML data are utilised.

The fitting parameters (a and b) of the BT-to-$\langle RH\rangle$ retrieval are determined once using a representative dataset of thermodynamic profiles and sampling the satellite field of view (see Sect. 2). This training database is composed of temperature (T) and specific humidity (q) profiles extracted from ERA-Interim. The ERA-Interim training database is composed of clear sky only profiles covering the years 2001, 2006 and 2007 and of samples of the seasonal cycle with the 1st day of the months of January,

Full Screen / Esc

Printer-friendly Version

Interactive Discussion

April, July and October of each year (4 time steps per day). The clear sky is defined using the ERA-Interim cloud fraction with a strict value of 0 at all levels. In addition to the cloud screening, a quality check is performed onto the relative humidity profiles (determined with respect to the water phase only) to remove the driest cases where the relative humidity reaches values below 1 % in the free troposphere, and also to remove the saturated profiles (> 100 %). Roca et al. (2009) determined $a = -0.1248$ and $b = 33.46$.

The identification of clear sky and low level clouds relies on ISCCP-DX data, and the FTH quality depends on the cloud classification quality. Strongest quality degradation can be expected when high level clouds are not correctly identified. For data until February 1997 coastal areas exhibit spurious quality due to issues in cloud detection. Also, the retrieval is not reliable over elevated terrain with surface pressures less than 700 hPa because the observed signal might contain contributions from the surface.

An assessment of the literature provides several definitions of the vertical averaging operator $\langle \cdot \rangle$ involved in the definition of FTH, according to the interpretation of the observed radiation (Brogniez et al., 2009):

 – idealized Jacobian $\Delta BT/\Delta RH$ whose weights are defined in temperature coordinates (e.g. Soden and Bretherton, 1993, 1996),

 – local relative humidity Jacobian $J_{RH} = \partial BT/\partial RH$ (e.g. Roca et al., 2003; Brogniez, 2004; Brogniez et al., 2004),

 – transmission-derived weighting function $\partial \tau / \partial \ln(p)$ (e.g. Schmetz and Turpeinen, 1988; Stephens et al., 1996).

The selection of the most adapted operator for the retrieval is based on a comparison between the three regressions defined from the three definitions of FTH, using ERA40 data. Figure 2 illustrates the results of this evaluation with scatter plots of the bias between the weighted relative humidity profiles ("observed") and the computed FTH using simulated BTs ("retrieved") and the "observed" FTH. The statistics provided in

Fig. 2 clearly highlight the better quality of the fit obtained with J_{RH}, and thus the more precise definition of the FTH. An analysis of the differences in spatial distributions of the peak height of the three different averaging operators (Roca et al., 2009) also shows that the spatial distribution of the peak heights resembles the spatial distribution of relative humidity when using J_{RH} and the transmission-derived weighting function. The latter, however, exhibits a bimodal distribution which is not present in J_{RH} results.

Thus, FTH is defined as the mean relative humidity weighted by J_{RH}, normalized by the sum of weights. In practice, the layer between 150 and 700 hPa is considered in the computation of the FTH:

$$FTH(RH) = \frac{\sum\limits_{p=700\,hPa}^{150\,hPa} RH(p) \times J_{RH}(p)}{\sum\limits_{p=700\,hPa}^{150\,hPa} J_{RH}(p)}. \tag{3}$$

with RH(p) defined between 0 and 100 %, with respect to liquid phase of water.

The retrieval was applied to Meteosat-2–5 and Meteosat-7–9 and provides relative humidity values within ±45° longitude and ±45° latitude. FTH is available at 3 hourly temporal resolution and as monthly averages (straightforward averages over all valid observations) on a regular latitude/longitude grid with a spatial resolution of 0.625° × 0.625°. The temporal coverage of the data set ranges from July 1983 to December 2009. For the reasons given in Brogniez et al. (2009) the Meteosat-6 period from March 1997–May 1998 is not covered.

From now on relative and absolute units are given in % and %RH, respectively.

Figure 3 shows exemplary instantaneous and monthly average products, and Fig. 4 illustrates full time series seasonal averages. Strong minima in FTH over northern and southern Africa during boreal summer as well strong maxima in FTH at the Inter Tropical Convergence Zone (ITCZ) are evident. Maxima in FTH and extent and strength of dry areas are a function of season. For the three regions illustrated in Fig. 4 the

time series of FTH averages are shown in Fig. 5. The three time series exhibit strong differences in amplitude and shape of the annual cycle. Note that minor changes in the definition of the regions have a noticeable impact on the time series, in particular also on outliers. Such outliers seem to be caused by deviations from the climatological behaviour of atmospheric dynamics on regional scale.

5 Towards an uncertainty budget estimate

This section briefly discusses the uncertainty budget estimate for the FTH product. The uncertainty budget is composed of three main uncertainty source terms following Chambon et al. (2012): (1) calibration uncertainty, (2) retrieval uncertainty and (3) sampling uncertainty. In line with Roca et al. (2012b) the calibration uncertainty is considered to be a systematic difference while the retrieval uncertainty varies along the design of the algorithm. The representativeness uncertainty depends on the space/time accumulation and vanishes at the instantaneous pixel scale. This uncertainty depends on the number of independent observations. In order to estimate this number the correlation length in space and time for FTH has been estimated by analysing variograms (see Roca et al., 2012 for details).

We consider an upper bound calibration uncertainty of 1 K (van de Berg et al., 1995). In this case, the relative uncertainty on FTH is equivalent to the intercept of the retrieval (b in Eq. 2) and is between 10 and 15 % (Roca et al., 2012b). Results from the training of the FTH retrieval allow the estimation of the retrieval uncertainty. Based on the tropical training RMSD = 2 %RH (8 % when assuming an average FTH of 25 %) and an average difference of 0.3 %RH were estimated. Assuming a daily average over a 2.5° grid box and a typical standard deviation of 20 % would yield to a 10 % relative sampling uncertainty. As a result, in this idealized case, the total uncertainty on the FTH mean is driven equally by the calibration and sampling terms and less so by the algorithm term. The estimated total uncertainty is the square root of the sum of the three variances and in this case is around 16–19 % at one sigma (Roca et al., 2012).

Title Page

Abstract | Introduction

Conclusions | References

Tables | Figures

|◄ | ►|

◄ | ►

Back | Close

Full Screen / Esc

Printer-friendly Version

Interactive Discussion

6 Evaluation

6.1 Data record for evaluation

The ARSA version 2.7 has been developed and provided by the Atmospheric Radiation Analysis group at Laboratoire de Météorologie Dynamique (LMD), Paris, France. In a first processing step, the worldwide distributed radiosonde stations are quality controlled. E.g., water vapour observations are considered only when available up to a pressure of 350 hPa at minimum, and the Thermodynamic Initial Guess Retrieval (TIGR, also developed at LMD) climatological data base is used to remove outliers. In a second step existing radiosonde measurements are combined with other reliable data sources. This step depends on ERA-Interim data, which are also used for extrapolation into upper levels of the atmosphere. Finally, the profiles are interpolated to the 43 pressure levels of the radiative transfer model 4A (Automatized Atmospheric Absorption Atlas; Scott and Chedin, 1981). ARSA covers the period 1979 to early 2011 with a few 10 000 observations per month. More details can be found under http://ara.abct.lmd.polytechnique.fr/index.php?page=arsa.

In previous studies the CSR quality has been evaluated using a previous version of ARSA data (Brogniez et al., 2006, 2009) showing high quality and stability of the CSR data over the period 1983–2005.

6.2 Methodology

The evaluation approach using ARSA follows the approach given in Brogniez et al. (2006, 2009). In order to simulate Meteosat-5 observations RTTOV 9.3 has been applied to ARSA. RTTOV (Radiative Transfer for the TIROS Operational Vertical Sounder, Matricardi et al., 2004) uses fast transmittance algorithms based on accurate transmittances obtained by line-by-line computations (GENLN2 for the 3–20 μm spectral range, Edwards, 1992), and is thus dependent on the spectroscopic database (HITRAN-2000, Rothman et al., 2003). For the specific case of the 6.3 μm

strong vibration-rotation absorption band by water vapour, the RTTOV model takes into account the water vapour continuum (foreign-broadening and self-broadening, model CKD-2.4, Clough et al., 1989) that has a non-negligible contribution in the water vapor band, and that has been shown to be of the same order of magnitude as the calibration
5 uncertainties ($\sim$ 2 K, e.g. Stephens et al., 1996, Soden et al., 2000). When looking at the work of Brunel and Turner (2003) which is referenced in the RTTOV v9 user guide the uncertainty of RTTOV with respect to the Meteosat water vapour channel is < 0.1 K in bias with a standard deviation of > 0.3 K.

RTTOV also provides various standard Jacobians. These are converted to Jacobians
10 with respect to relative humidity, which is used for integration of ARSA data to be consistent with FTH from Meteosat. The region within ±45° N/S and ±45° E/W and the period July 1983-December 2009 is considered for the comparison against ARSA.

The following selection criteria are applied during validation:

– night time only to avoid potentially remaining issues with radiosonde quality in the
15   upper troposphere,

– FTH > 5 % so that potential surface contributions are reduced,

– absolute BTs differences < 3 K and simulated and observed BTs > 220 K in order to minimise cloud detection uncertainties.

Two pairs of ARSA and Meteosat observations are considered as collocated when
20 the temporal and spatial distances are within 1.5 h and 0.625°, respectively. Though ARSA also contains measurements from radiosondes on ships and small islands the validation is dominated by observations over land.

As uncertainty parameters the systematic relative difference, here relative bias, the corresponding root mean square difference (RMSD, bias corrected) and the decadal
25 stability are determined on a monthly basis and as spatial averages. The uncertainty parameters are only considered when the number of valid observations is larger than 10.

6.3 Results

The time series of monthly averages of absolute and relative bias, absolute and relative RMSD and number of valid observations N are shown in Fig. 6. The time series averages of relative bias, relative RMSD and N are −3.2, 16.8 and 170 %, respectively. 55 % of the monthly relative biases and the full time series average relative bias are smaller than the GCOS requirement. The relative bias exhibits strong temporal fluctuations and a standard deviation of 4.5 %. Also, N strongly fluctuates in time but neither small nor large values of N systematically coincide with maxima/minima in relative bias. The temporal correlation between N and the relative bias is −0.01. Besides several local maxima and minima in bias the following features are evident:

– increase in relative bias between summer 1988 and summer 1990,

– maximum in relative bias in January 1996, with generally spurious biases in 1996.

These features likely originate from changes in calibration procedures or instrumentation, as it has been discussed in Sect. 3. The main difference is that the observed features appear enhanced in the relative FTH bias due to the exponential relation between CSR and FTH and to the normalisation. Also, sharp summer minima in the relative bias are visible frequently. These minima are less evident prior to 2001. The sharp minima in the relative bias during summer are likely caused by increased uncertainties in the FTH retrieval in presence of small FTH values. The RMSD exhibits less strong variations than the relative bias and a slight decrease over time between 1988 and 2006. More than 66 % of the monthly RMSD values are within 16–19 %, which is the above estimated uncertainty of the FTH product.

The time series averages of absolute bias and RMSD (Fig. 6, third panel) are −1.2 %RH and 5.0 %RH, respectively. The majority of the features are similar as in the relative bias and RMSD plots but appear damped. The most obvious difference is the missing decrease in RMSD. It seems that the absolute RMSD and bias are stable over time and that the normalisation to FTH causes the decrease in relative RMSD, an

indication for a general increase in FTH. Note that the normalisation is done relative to FTH from ARSA. It also seems that the annual cycle of the absolute bias is less pronounced. The normalisation amplifies the annual cycle because the months of July and August exhibit strongest minima and largest areas of dry regions.

We also evaluated the scatter plot and the difference histogram of FTH from Meteosat and FTH from ARSA (not shown). In both plots a small bias between both FTH data records is obvious with the ARSA based FTH values being larger than the Meteosat based FTH values. The histogram of the differences peaks at -1 ± 1 %RH and is slightly skewed to negative values.

We consider stability to be the slope of the linear regression fitted to the monthly mean difference between the FTH product and the corresponding ARSA data. Based on the differences shown in Fig. 6 (top panel) and after conversion from % month^{-1} into % year^{-1}, we found the decadal stability to be 0.5 ± 0.45 % which envelopes the GCOS requirement of 0.3 % (GCOS-154). The uncertainty of the decadal stability is relatively large and is directly evident in Fig. 6.

7   Variability and trend analysis

In this section we discuss results from first applications in the field of climate analysis. After an introduction of the frequency of occurrence of FTH < 10 % (FTHp10) we focus on the analysis of the standard deviation on inter-annual scale, the correlation to the El Niño 3.4 and the Quasi-Biennial Oscillation (QBO) indices and differences in decadal averages between the 1990s and 2000s. Beyond a general scientific interest in results related to the above analysis it is also a valuable effort for the discussion of linear trends and associated uncertainties in Sect. 7.3.

Throughout this section, full years are considered, that is, the period January 1984– December 2009.

7.1 FTHp10

Roca et al. (2012a) introduced the frequency of occurrence of dry air as a marker of the behaviour of the dry part of the PDF of FTH, namely the frequency of occurrence of FTH < 10 %, noted as FTHp10. On the top of corresponding to the radiatively sensitive range of FTH, such a climatological indicator is more resilient to the various assumptions in the retrieval (like cloud clearing). Through a stronger contrast between minima and maxima it also better reveals the spatial distribution of the moisture field as seen in the FTHp10 seasonal climatology shown in Fig. 7. The frequently dry areas strongly coincide with the dry seasonal averages in Fig. 4. It further reveals the dry area in the Southern tropical Atlantic Ocean that witnesses very dry air more than 70 % of the time all year through, and it highlights the strong maxima in FTHp10 in value and in spatial extend that take place in boreal summer in comparison with the other seasons. The uniqueness of the dry northeastern Mediterranean Sea region (Brogniez et al., 2009) is strongly evident in the boreal summer climatology.

7.2 Variability

Though persistent dry and wet areas in FTH and FTHp10 seem to be present in space and in time the variability is nevertheless large on various temporal scales. Therefore, an analysis of the variability of FTH and FTHp10 is in itself valuable to guide conclusions on basis of averages of FTH and FTHp10 alone. In addition, we will assess the significance of trends in FTH and FTHp10 in the next section. The confidence probability is a function of standard deviation and therefore variability. Hence, we analyse the spatial distribution of the standard deviation on inter-annual scale, the correlation to ENSO and QBO indices and the differences on the decadal scale.

Figure 8 shows the relative standard deviation in FTH and in FTHp10 per season in order to assess the interannual variability. The maxima in relative standard deviation in FTH are found over the South and North Atlantic and over central-east Africa as well as over northeast Africa in DJF and JJA, respectively. Minima are associated with the

Title Page

Abstract | Introduction

Conclusions | References

Tables | Figures

◄ | ►►

◄ | ►

Back | Close

Full Screen / Esc

Printer-friendly Version

Interactive Discussion

ITCZ and the extratropics. Noticeable is that SON exhibits clearly the minimum relative standard deviation, mainly through largely reduced maxima. Obviously the positions of maxima/minima in relative standard deviation frequently coincide with the position of minima/maxima in FTH but also with gradient areas between dry and wet regions. These results are in large agreement with the findings of Brogniez et al. (2009). We recall here the outstanding relevance of variability in dry FTH on outgoing longwave radiation (e.g., Udelhofen and Hartman, 1995; Sohn and Schmetz, 2004). When keeping in mind that minima in FTH are associated with maxima in FTHp10, similar findings are found for FTHp10, but only for the dry end of the PDF. Also, the strong maximum in the core area of the region in north east Africa in JJA in relative standard deviation of FTH appears as a local minimum in standard deviation of FTHp10, indicating a strong stability of the occurrence of dry events in this region

Following Roca et al. (2012a) large-scale dynamics have a strong impact on the distribution and variability of FTH. For the dry region over northeast Africa in JA Brogniez et al. (2009) showed that the dry composite has its origin mainly in the tropics but with significant contributions from the extratropics as well. The wet air mainly originates from the tropics only. When looking at the specific feature in FTHp10 over the north east Africa in JJA not only absolute values and their variability are important features but also the variability of their extent and position should be analysed to better understand the overall dynamics and underlying FTH distributions, their impact on OLR and changes over time.

The Pearson's correlation coefficient between seasonal averages of FTH as well as FTHp10 and the El Niño 3.4 index (available from http://www.esrl.noaa.gov/psd/data/climateindices/list/) has been analysed on grid basis (not shown). In this analysis, only seasonal averages for DJF have been considered because El Niño events are more intense during boreal winter. The confidence probability of the correlation has been computed as described in Shi et al. (2013). We found average positive and negative correlations of around ± 0.15 and that the area fraction with a confidence probability of 95 % or larger are 1.8 and 3.6 % for FTH and FTHp10, respectively. FTH and FTHp10

exhibit significant correlations over northeast Africa and parts of the Arabian Peninsula, with FTH/FTHp10 values being positively/negatively (0.48/-0.45) correlated with the El Niño 3.4 index. The positive correlation for FTH is consistent with results of Shi et al. (2013) who analysed the correlation between BT based on HIRS observations and the El Niño 3.4 index. A joint analysis of correlations between satellite based FTH data records and several climate indices will be conducted within G-VAP. Similarly, the correlation of deseasonalised FTH and FTHp10 values to the Quasi-Biennial Oscillation (QBO) index has been analysed. The total area fraction of significant correlation is slightly larger than for the correlation to the El Niño 3.4 index but with associated average correlations around 0.13 only. We conclude that El Niño and QBO have minor contributions to the overall variability in FTH and FTHp10 over the considered area.

The FTH data record covers two full decades, namely the 1990s and the 2000s. In Fig. 9 the differences in decadal averages of FTHp10 between the 1990s and the 2000s are shown per season. Negative values occur when the 2000s exhibit larger FTHp10 values than the 1990s, that is, dry events would be more frequent in the 2000s. Obviously, FTHp10 is generally larger in the 2000s than in 1990s. The maximum and minimum area fractions of negative differences are 90 % (DJF) and 71 % (SON), respectively. The regions of minimum difference mainly coincide with gradient areas between dry and wet regions and to a lower extent with dry regions. The largest connected area of positive differences is found over north east Africa in SON and is located at the west-south-west border of a regional maximum in FTHp10. This probably corresponds to an east-north-east retreat of the dry region between the 1990s and 2000s. In order to assess the significance of the differences the ratio of these differences to the square root of the squared sum of the internal decadal standard deviations were analysed (not shown). The maximum and minimum area fractions with absolute ratios larger than one are 9 % (DJF) and 1 % (SON), respectively. Areas of large absolute ratios are typically found between ITCZ and neighbouring dry areas. Though nearly the full area of interest exhibits an increase in the frequency of dry values we cannot conclude that this tendency is significant.

7.3 Linear trend analysis

7.3.1 Methodology

We tested two different methods for the analysis of linear trends: "median of pair wise slopes regression" or "Theil–Sen slope estimator" (Theil, 1950) and linear regression. In principle, the "Theil–Sen slope estimator" method is more robust, i.e. less sensitive to outliers, than linear regression and hence better suited for analysis of linear trends in climatological data series. This estimator takes the median of all pair wise slopes in the data. In order to accurately estimate confidence probabilities approximately 600 pairs are needed (Wilcox, 2001) instead of the 312 that we have in the FTH data record. Hence we have also used a simple linear regression computation. A comparison of the trend results exhibit minor differences in absolute values and patterns only (not shown). We therefore applied the linear regression method in the following. The estimated uncertainty of the trend is computed as described in Wilks (2011). Here, the autocorrelation is neglected because seasonal averages are considered. Based on the estimated uncertainty the confidence probability is computed with a two-sided Student's t test.

To increase the accuracy of the trend analysis we used $5° \times 5°$ averages instead of the full resolution of the original product.

7.3.2 Results

Figures 10 and 12 show the linear trend in FTH and FTHp10 and associated confidence probabilities per season for the period 1984–2009. Positive/negative trends in FTH largely coincide with negative/positive trends in FTHp10. An exception is the negative trend in FTH over southeast Europe in DJF where FTHp10 exhibits trends which are around $0\,\%\,year^{-1}$. Note that FTHp10 reflects only the very dry events while FTH has been average over the full range of FTH values.

In general and for both parameters strongest trends are observed in gradient areas between dry and wet regions and dry areas. The dipole structure of positive and

negative trends in FTH and FTHp10 over north-east Africa in DJF and JJA are located at the borders of the associated dry regions and can be an indication of a displacement of (frequently) dry regions in these areas. The observed trends in FTH and FTHp10 are hardly significant at the 95 % confidence level. The maximum/minimum area fractions with significant trends at such levels are 2.5 % (SON) and 19.8 % (MAM), both found for FTHp10. Largest connected areas of significant trends are found in the extra-tropics, coincide with generally large/small values of FTH/FTHp10 and small estimated uncertainties and should be interpreted with care as they are affected by potential oversimplifications of the retrieval scheme. The estimated uncertainties are shown in Figs. 11 and 13 for FTH and FTHp10, respectively. Areas of large absolute trends frequently coincide with large estimated uncertainties but also appear slightly displaced relative to the maxima in estimated uncertainty. Exceptions are an area of negative trends in FTH over Brazil and the neighbouring South Atlantic in SON. When comparing Fig. 11 and 13 with Fig. 8 the strong coincidence between the estimated uncertainty and the interannual variability becomes obvious. Thus, the interannual variability dominates the estimated uncertainty. This together with the temporal length of the record (26 years) explains that significant trends in FTH and FTHp10 are hardly observed in this analysis. In view of the work of Roca et al. (2012a) who analysed changes in FTHp10 using climate model output it can be expected that observations need to be largely extended in time to allow for a verification of climate model output.

Brogniez et al. (2009) reported that 1985 was among the driest years of the full FTH data record. As it is located at the start of the time series it has a strong impact on the trend estimate. We exemplary assessed this impact for FTHp10 by removing the first two years from the data record (not shown). After recomputation of the trends, dry areas and gradient areas between dry and wet areas exhibit larger positive trends and connected areas of such trends cover larger areas. In particular, the dry area over northeast Africa in JJA and the dry area over the South Atlantic in DJF exhibit significant positive trends at the 95 % confidence level. Interestingly the areas of significant trends in the extratropics in MAM and over central Africa in DJF almost vanish which is

associated with trends being closer to zero. As stated in Santer et al. (2011) we again confirm that trend estimates, their significance and uncertainty depend on the considered period and in particular on the statistics of the data at start and end of the time period.

⁵   Though the estimated trends and the differences between decadal averages of FTHp10 from the 1990s and the 2000s are practically not significant and cover different periods, the spatial patterns of increasing FTHp10 values generally coincide with negative differences. Moreover, the results nevertheless fit in the big picture evocated in the introduction section. It would be interesting to see if trends in dry areas, in partic-

¹⁰ ular for FTHp10 are replicated in back trajectory based relative humidity constructions to see if such an increase is related to a change in the large scale dynamics of the last saturations statistics. In this context the dipole structures of positive and negative FTH and FTHp10 trends over north east Africa in JJA and DJF are remarkable. The associated feature in the estimated uncertainty coincides with a similar feature in interannual

¹⁵ variability. Though the trends are hardly significant, this speaks for an extension of the back trajectory analysis by an analysis of the position and extend of the dry areas, specifically in north east Africa.

8   Conclusions

Meteosat-2 to Meteosat-5 and Meteosat-7 to Meteosat-9 observations at 6.3 µm are

²⁰ used to retrieve information on humidity in the free troposphere. The inversion from BT to FTH is reliable in the clear sky case and in the presence of low level clouds. Temperature data from ERA-Interim is used as well to slightly improve the performance of the statistical retrieval scheme. Within a successful cooperation between a research institute and an operational service the FTH data record was extended into the SEVIRI

²⁵ era. The FTH data record is now released free of charge under https://www.cmsaf.eu/wui and is reference under doi: 10.5676/EUM_SAF_CM/FTH_METEOSAT/V001. The FTH data record is available within ±45° N/S and ±45° E/W with a spatial resolution of

0.625°, and it covers the years 1983–2009 with a temporal resolution of 3 h. Monthly averages are also available.

Based on the comparison against FTH derived from the ARSA archive by using relative humidity Jacobians for integration of the ARSA profiles, the average relative bias and relative RMSD are −3.2 and 16.8 %, respectively. The relative RMSD is in agreement with the estimated uncertainty. The decadal stability is 0.5±0.45 %. The relatively large uncertainty estimate envelopes the GCOS requirement on humidity in the free troposphere of 0.3 % per decade. Due to the increase in bias between summer 1988 and summer 1990 and a maximum in bias in January 1996, with generally spurious biases in 1996, and though significant efforts have been dedicated to the homogenisation of the Meteosat time series, the quality of the FTH data record will benefit from a Fundamental Climate Data Record (FCDR) of the full Meteosat time series, including the recovery of Meteosat-6 data in order to close data gaps in the time series.

As exemplary applications we have analysed the inter-annual relative standard deviation, differences between decadal averages of the 1990s and 2000s and linear trends using seasonal averages of FTH and FTHp10. Obviously, maxima in inter-annual standard deviations generally coincide with minima in FTH and maxima in FTHp10. Maxima in absolute estimates of the trends in seasonal FTH and FTHp10 are accompanied by maxima in standard deviation, and in consequence, the estimated trends are hardly significant. In the ITCZ environment where the results could be corrupted by the cloud-clearing method, the trends and their uncertainties should be interpreted with caution. However, the maxima in trend estimate of FTHp10 coincide with maximum absolute differences in decadal averages of FTHp10 of 1990s and 2000s. In the dry free tropospheric subtropical regions the linear analysis results, though not significant, are consistent with theoretical considerations, in both the sign and the small magnitude of the change over the last ∼ 25 years. The combined presentation of trend estimates, confidence probability and estimated uncertainty are valuable information for further analysis of changes in the climate system. We conclude that the analysis of the dry end of the FTH distribution is of very large relevance not only because of its impact

on OLR but also because of the observed indication of small changes in value, in area and the associated large variability.

Again, the analysis will strongly benefit from the availability of a Meteosat FCDR and a gap-free input data record. Of equal importance is the extension of the temporal coverage to the most recent times in order to promote a robust view on the decadal changes estimated here using linear trends computations. Within WMO's SCOPE-CM initiative EUMETSAT leads the activity on the "Inter-calibration of imager observations from time-series of geostationary satellites (IOGEO)". Among others, this activity aims at the development and provision of a Meteosat FCDR. This FCDR will be used to improve the quality of the Meteosat based FTH data record.

Initial comparisons to other available FTH/UTH data record, e.g., based on HIRS and AMSU-B observations have been carried out already by CM SAF (http://www.cmsaf.eu/docs) and by the GEWEX water vapor assessment (G-VAP, http://www.gewex-vap.org). Among others, UTH data and inter-comparisons to other freely available UTH data records are among the objectives of G-VAP. The work presented here is part of the analysis of long-term temporal changes within G-VAP. The extension of this analysis to other UTH data records and the inter-comparison is work in progress by an international team associated with G-VAP, with final results expected by the end of 2015.

References

Bréon, F.-M., Jackson, D. L., and Bates, J. J.: Calibration of the Meteosat water vapor channel using collocated NOAA/HIRS 12 measurements, J. Geophys. Res., 105, 11925–11933, 2000.

5 Brogniez, H., Roca, R., and Picon, L.: Evaluation of the distribution of subtropical Free Tropospheric Humidity in AMIP-2 simulations using Meteosat water vapor channel data Geophys. Res. Lett., 32, L19708, doi:10.1029/2005GL024341, 2005.

Brogniez, H., Roca, R., and Picon, L.: A clear sky radiances archive from Meteosat "water vapor" observations, J. Geophys. Res., 111, D21109, doi:10.1029/2006JD007238, 2006.

10 Brogniez, H., Roca, R., and Picon, L.: A study of the free tropospheric humidity interannual variability using Meteosat data and an advection–condensation transport model, J. Climate, 22, 6773–6787, 2009.

Brogniez, H., Clain, G., and Roca, R.: Upper Tropospheric Humidity from SAPHIR/Megha-Tropiques: algorithm overview and validation against tropical soundings, JAMC, submitted, 2014.

15 Brunel, P. and Turner, S.: On the use of Planck-weighted transmittances in RTTOV, presented at the 13th International TOVS Study Conference, Ste Adele, Canada, 29 October–4 November, 2003.

Buehler, S. A. and John, V. O.: A simple method to relate microwave radiances to upper tropospheric humidity, J. Geophys. Res., 110, D02110, doi:10.1029/2004JD005111, 2005.

20 Buehler, S. A., Kuvatov, M., John, V. O., Milz, M., Soden, B. J., Jackson, D. L., and Notholt, J.: An upper tropospheric humidity data set from operational satellite microwave data, J. Geophys. Res., 113, D14110, doi:10.1029/2007JD009314, 2008.

Chambon, P., Jobard, I., Roca, R., and Viltard, N.: An investigation of the error budget of tropical rainfall accumulation derived from merged passive microwave and infrared satellite measure-

25 ments, Q. J. Roy. Meteor. Soc., doi:10.1002/qj.1907, 139, 879–893, 2012.

Clough, S., Kneizys, F., and Davies, R.: Line shape and the water vapor continuum, Atmos. Res., 23, 229–241, 1989.

Dee, D. P., Uppala, S. M., Simmons, A. J., Berrisford, P., Poli, P., Kobayashi, S., Andrae, U.,

30 Balmaseda, M. A., Balsamoa, G., Bauer, P., Bechtold, P., Beljaars, A. C. M., van de Berg, L., Bidlot, J., Bormann, N., Delsol, C., Dragani, R., Fuentes, M., Geer, A. J., Haimberger, L., Healy, S. B., Hersbach, H., Holm, E. V., Isaksen, L., Kallberg, P., Köhler, M., Matricardi,

Climatology of free tropospheric humidity

M. Schröder et al.

Title Page	
Abstract	Introduction
Conclusions	References
Tables	Figures

⏮	⏭
◀	▶
Back	Close

Full Screen / Esc

Printer-friendly Version

Interactive Discussion

M., McNally, A. P., Monge-Sanz, B. M., Morcrette, J.-J., Park, B.-K., Peubey, C., de Rosnay, P., Tavolato, C., Thepaut, J.-N., and Vitart, F.: The ERA-Interim reanalysis: configuration and performance of the data assimilation system, Q. J. Roy. Meteor. Soc., 137, 553–597, 2011.

Durre, I., Vose, R. S., and Wuertz, D. B.: Overview of the integrated global radiosonde archive, J. Climate, 19, 53–68, 2006.

Edwards, D.: GENLN2: a general line-by-line atmospheric transmittance and radiance model, Tech. Rep., NCAR/TN-367, NCAR, Boulder, Colorado, USA 1992.

GCOS-154: Systematic Observation Requirements for Satellite-based Products for Climate, Supplemental details to the satellite-based component of the Implementation Plan for the Global Observing System for Climate in Support of the UNFCCC (Update), December 2011, WMO, Geneva, Switzerland, 2011.

Held, I. M. and Soden, B. J.: Water vapor feedback and global warming, Annu. Rev. Energ. Env., 25, 441–475, 2000.

Hurley, J. V. and Galewsky, J.: A last-saturation diagnosis of subtropical water vapor response to global warming, Geophys. Res. Lett., 37, L06702, doi:10.1029/2009GL042316, 2010.

Jackson, D. and Bates, J.: Upper tropospheric humidity algorithm assessment, J. Geophys. Res., 106, 32259–32270, 2001.

John, V. O., Holl, G., Allan, R. P., Buehler, S. A., Parker, D. E., and Soden, B. J.: Clear-sky biases in satellite infrared estimates of upper tropospheric humidity and its trends, J. Geophys. Res., 116, D14108, doi:10.1029/2010JD015355, 2011.

John, V. O., Holl, G., Atkinson, N., and Buehler, S. A.: Monitoring scan asymmetry of microwave humidity sounding channels using simultaneous all angle collocations (SAACs), J. Geophys. Res.-Atmos., 118, 1536–1545, doi:10.1002/jgrd.50154, 2013.

Köpken, C.: Monitoring of Meteosat WV Radiances and Solar Stray Light Effects, EUMET-SAT/ECMWF Fellowship Report No. 10, Reading, Berkshire, UK, 2001.

Matricardi, M., Chevallier, F., Kelly, G., and Thépaut, J.-N.: An improved general fast radiative transfer model for the assimilation of radiance observations, Q. J. Roy. Meteor. Soc., 130, 153–173, 2004.

Moradi, I., Buehler, S. A., John, V. O., and Eliasson, S.: Comparing upper tropospheric humidity data from microwave satellite instruments and tropical radiosondes, J. Geophys. Res., 115, D24310, doi:10.1029/2010JD013962, 2010.

Picon, L., Roca, R., Serrar, S., and Desbois, M.: A new METEOSAT "water vapor" archive for climate studies, J. Geophys. Res., 108, 4301, doi:10.1029/2002JD002640, 2003.

Climatology of free tropospheric humidity

M. Schröder et al.

Title Page

Abstract | Introduction

Conclusions | References

Tables | Figures

|◄ | ►|

◄ | ►

Back | Close

Full Screen / Esc

Printer-friendly Version

Interactive Discussion

Pierrehumbert, R. T., Brogniez, H., and Roca, R.: On the relative humidity of the atmosphere, in: The Global Circulation of the Atmosphere, edited by: Schneider, T. and Sobel, A. H., Princeton University Press, Princeton, New Jersey, USA, 143–185, 2007.

Roca, R., Brogniez, H., Picon, L., and Desbois, M.: Free Tropospheric Humidity observations from Meteosat water vapour channel data, Preprints, 17th Conf. on Hydrology, 8–13 February 2003, Long Beach, CA, American Meteorological Society, CD-ROM, J3.7, 2003.

Roca, R., Brogniez, H., Gif, N., and Picon, L.: Development of a consistent climatology of free tropospheric humidity employing observations from Meteosat satellites, EUMETSAT CM SAF Scientific and Technical Report, 23 October, Offenbach, Germany, 2009.

Roca, R., Chambon, P., Jobard, I., Kirstetter, P. E., and Gosset, M.: Comparing satellite and surface rainfall products over West Africa at meteorologically relevant scales during the AMMA campaign using error estimates, J. Appl. Meteorol. Clim., 49, 715–731, 2010.

Roca, R., Guzman, R., Lemond, J., Meijer, J., Picon, L., and Brogniez, H.: Tropical and extratropical influences on the distribution of free tropospheric humidity over the intertropical belt, Surv. Geophys., 33, 565–583, doi:10.1007/s10712-011-9169-4, 2012a.

Roca, R., Meijer-Fofana, J., Picon, L., and Brogniez, H.: Climatology of Free Tropospheric Humidity: Extension to SEVIRI, Error Analysis and Trend Assessment. EUMETSAT CM SAF Scientific and Technical Report, June 2012, Offenbach, Germany, 2012b.

Rossow, W. B. and Schiffer, R. A.: Advances in understanding clouds from ISCCP, B. Am. Meteorol. Soc., 80, 2261–2288, 1999.

Rothman, L. S., Barbe, A., Benner, D. C., Brown, L. R., Camy-Peyret, C., Carleer, M. R., Chance, K. V., Clerbaux, C., Dana, V., Devi, V. M., Fayt, A., Flaud, J.-M., Gamache, R. R., Goldman, A., Jacquemart, D., Jucks, K. W., LaMerty, W. J., Mandin, J.-Y., Massie, S. T., Nemtchinov, V., Newnham, D. A., Perrin, A., Rinsland, C. P., Schroeder, J., Smith, K. M., Smith, M. A. H., Tang, K., Toth, R. A., Vander-Auwera, J., Varanasi, P., and Yoshino, K.: The HITRAN molecular spectroscopic database: edition of 2000 including updates through 2001, JQSRT, 82, 5–44, 2003.

Santer, B. D., Mears, C., Doutriaux, C., Caldwell, P., Gleckler, P. J., Wigley, T. M. L., Solomon, S., Gillett, N. P., Ivanova, D., Karl, T. R., Lanzante, J. R., Meehl, G. A., Stott, P. A., Taylor, K. E., Thorne, P. W., Wehner, M. F., and Wentz, F. J.: Separating signal and noise in atmospheric temperature changes: the importance of timescale, J. Geophys. Res., 116, D22105, doi:10.1029/2011JD016263, 2011.

Climatology of free tropospheric humidity

M. Schröder et al.

Title Page

Abstract | Introduction

Conclusions | References

Tables | Figures

◀ | ▶

◀ | ▶

Back | Close

Full Screen / Esc

Printer-friendly Version

Interactive Discussion

Schmetz, J., Geijo, C., Menzel, W. P., Strabala, K., van de Berg, L., Holmlund, K., and Tjemkes, S.: Satellite observations of upper tropospheric relative humidity, clouds and wind field divergence, Beitr. Phys. Atmos., 68, 345–357, 1995.

Scott, N. A. and Chedin, A.: A fast line-by-line method for atmospheric absorption computation: the Automated Atmospheric Absorption Atlas, J. Appl. Meteorol., 20, 802–812, 1981.

Sherwood, S. C., Roca, R., Weckwerth, T., and Andronova, N.: Tropospheric water vapor, convection and climate, Rev. Geophys., 48, RG2001, doi:10.1029/2009RG000301, 2010a.

Sherwood, S. C., Ingram, W., Tsushima, Y., Satoh, M., Roberts, M., Vidale, P. L., and O'Gorman, P. A.: Relative humidity changes in a warmer climate, J. Geophys. Res., 115, D09104, doi:10.1029/2009JD012585, 2010b.

Shi, L. and Bates, J. J.: Three decades of intersatellite-calibrated High-Resolution Infrared Radiation Sounder upper tropospheric water vapor, J. Geophys. Res., 116, D04108, doi:10.1029/2010JD014847, 2011.

Shi, L., Schreck III, C. J., and John, V. O.: HIRS channel 12 brightness temperature dataset and its correlations with major climate indices, Atmos. Chem. Phys., 13, 6907–6920, doi:10.5194/acp-13-6907-2013, 2013.

Soden, B. and Bretherton, F.: Upper tropospheric relative humidity from the GOES 6.7 ìm channel: method and climatology for July 1987, J. Geophys. Res., 98, 16669–16688, 1993.

Soden, B. J. and Bretherton, F. P.: Interpretation of TOVS water vapor radiances in terms of layer average relative humidities: method and climatology for the upper, middle, and lower troposphere, J. Geophys. Res., 101, 9333–9343, doi:10.1029/96JD00280, 1996.

Engelen, R., Garand, L., Jackson, D., Jedlovec, G., Kleespies, T., Randel, D., Rayer, P., Salathe, E., Schwarzkopf, D., Scott, N., Sohn, B., de Souza-Machado, S., Strow, L., Tobin, D., Turner, D., van Delst, P., and Wehr, T.: An intercomparison of radiation codes for retrieving upper-tropospheric humidity in the 6.3 µm band: a report from the first GvaP workshop, B. Am. Meteorol. Soc., 81, 797–808, 2000.

Soden, B. J., Wetherald, R. T., Stenchikov, G. L., and Robock, A.: Global cooling after the eruption of Mount Pinatubo: a test of climate feedback by water vapor, Science, 296, 727–730, 2002.

Sohn, B. J. and Schmetz. J.: Water vapor-induced OLR variations associated with high cloud changes over the tropics: a study from meteosat-5 observations, J. Climate, 17, 1987–1996, 2004.

Spencer, R. and Braswell, W. D.: How dry is the tropical free troposphere? Implications for global warming theory, B. Am. Meteorol. Soc., 78, 1097–1106, 1997.

Stephens, G., Jackson, D., and Wittmeyer, I.: Global observations of upper tropospheric water vapor derived from TOVS radiance data, J. Climate, 9, 305–326, 1996.

Theil, H.: A rank-invariant method of linear and polynomial regression analysis, Nederl. Akad. Wetensch. Proc., 53, 386–392 (part I), 521–525 (part II), 1397–1412 (part III), 1950.

Udelhofen, P. M. and Hartmann, D. L.: Influence of tropical cloud systems on the relative humidity in the upper troposphere, J. Geophys. Res., 100, 7423–7440, 1995.

Uppala, S. M., Kallberg, P. W., Simmons, A. J., Andrae, U., Da Costa Bechtold, V., Fiorino, M., Gibson, J. K., Haseler, J., Hernandez, A., Kelly, G. A., Li, X., Onogi, K., Saarinen, S., Sokka, N., Allan, R. P., Andersson, E., Arpe, K., Balmaseda, M. A., Beljaars, A. C. M., Vande Berg, L., Bidlot, J., Bormann, N., Caires, S., Chevallier, F., Dethof, A., Dragosavac, M., Fisher, M., Fuentes, M., Hagemann, S., Holm, E., Hoskins, B. J., Isaksen, L., Janssen, P. A. E. M., Jenne, R., McNally, A. P., Mahfouf, J.-F., Morcrette, J.-J., Rayner, N. A., Saunders, R.W., Simon, P., Sterl, A., Trenberth, K. E., Untch, A., Vasiljevic, D., Viterbo, P., and Woollen, J.: The ERA-40 re-analysis, Q. J. Roy. Meteor. Soc., 131, 2961–3012, 2005.

van de Berg, L. C. J., Schmetz, J., and Whitlock, J.: On the calibration of the Meteosat water vapour channel, J. Geophys. Res., 100, 21069–21076, 1995.

Wilcox, R. R.: Theil–Sen estimator, in: Fundamentals of Modern Statistical Methods: Substantially Improving Power and Accuracy, Springer, New York, USA, 207–210, 2001.

Wilks, D. S.: Statistical Methods in the Atmospheric Sciences, 3rd revised edn., Academic Press, San Diego, California, USA, 2011.
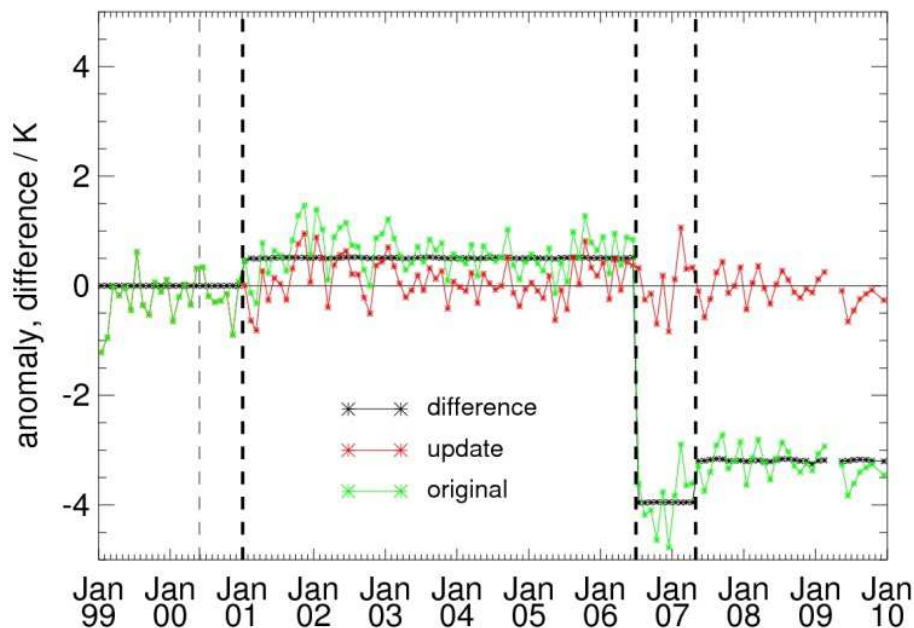
Fig. 1. Monthly deseasonalised clear sky brightness temperature anomaly for the original data (green) and the updated homogenised data (red). The black line shows the difference between both anomalies. The thick dashed vertical lines mark the time when homogenisation was applied and the thin dashed line marks the time when the black body calibration has been implemented.

Full Screen / Esc

Printer-friendly Version

Interactive Discussion
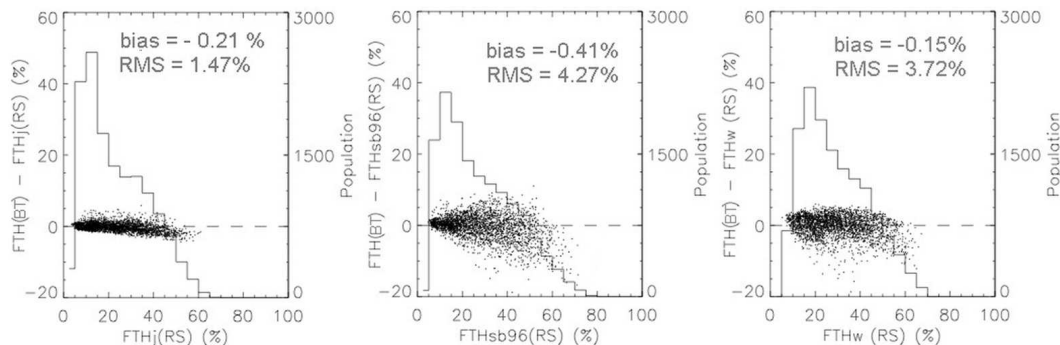
Fig. 2. Scatter plot of bias between "retrieved" FTH from simulated BT and "observed" FTH using the local Jacobian ("FTHj", left panel), the idealized Jacobian ("FTHsb96", middle panel) and the transmission-derived weighting function ("FTHw", right panel) and the "observed" FTH. ERA40 data of temperature and specific humidity was used as input. The histogram gives the "observed" FTH population, described on the right-hand side of the graphs. The average bias and RMS are also given.
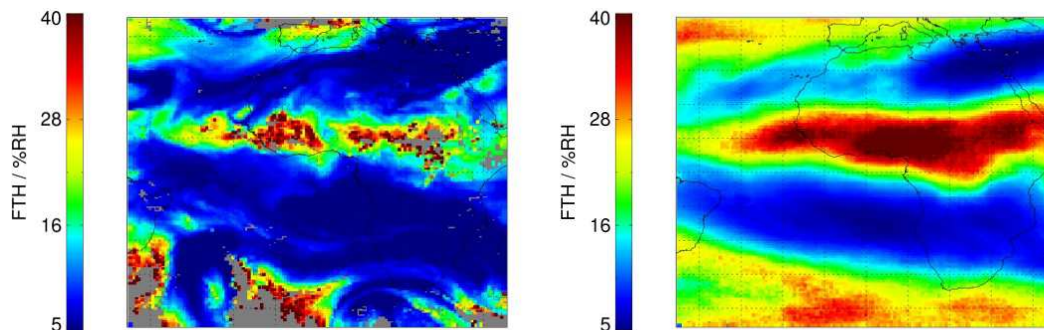
Fig. 3. Instantaneous FTH at 12:00 UTC on 15 July 2009 (left panel) and monthly averaged FTH for July 2009 (right panel). Undefined areas are marked grey and are usually associated to cloud top pressures above 700 hPa.
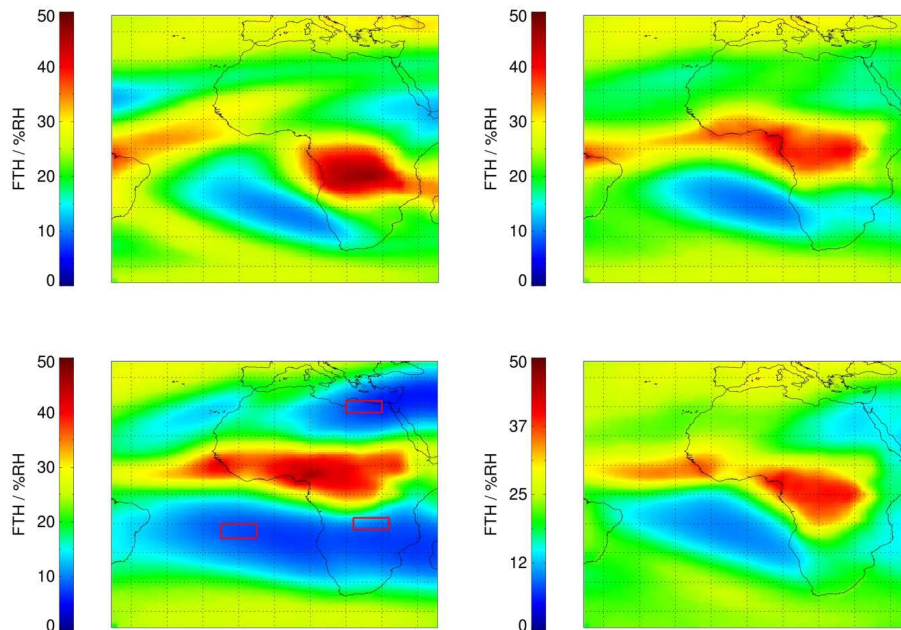
Fig. 4. Seasonal averages of FTH: December/January/February (top left), March/April/May (top right), June/July/August (bottom left) and September/October/November (bottom right). The considered period covers the years 1984–2009. The red boxes mark regions for which the average time series are plotted in Fig. 5.

Full Screen / Esc

Printer-friendly Version

Interactive Discussion
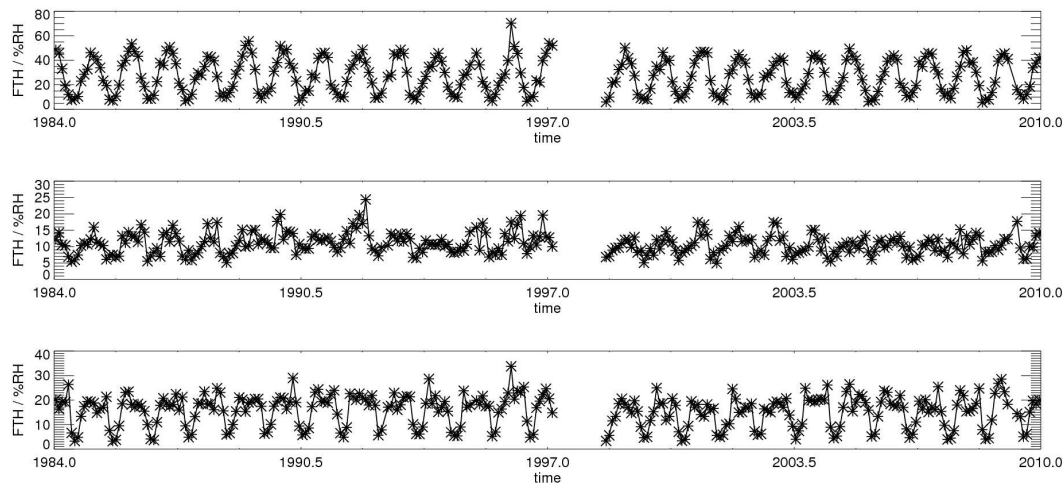
Fig. 5. Time series of regional averages over south central Africa (top), South Atlantic (middle) and north east Africa. The regions are shown in Fig. 4 (bottom left).
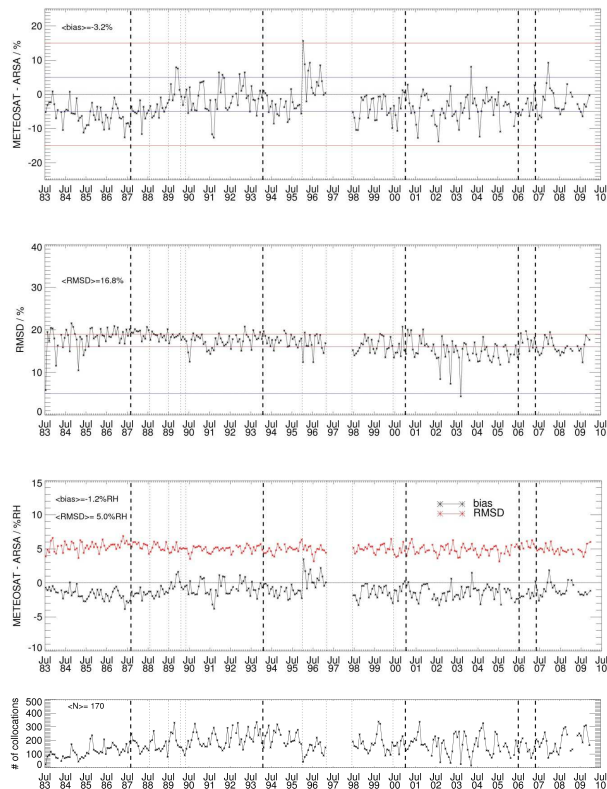
Fig. 6. Monthly mean of relative bias (top panel), relative RMSD (second panel), absolute bias and RMSD (third panel) and number of valid observations (N, bottom panel) between FTH from METEOSAT and FTH from ARSA. The thick dashed and the thin dotted lines mark homogenisation and major radiometric events. The time series averages of bias, RMSD and N are also given. The colored lines in the first two panels mark the FTH requirements from Global Climate Observing System (GCOS-154), the error budget estimate from Sect. 5 and a line at 15 % which is close to the peak value in maximum relative bias.
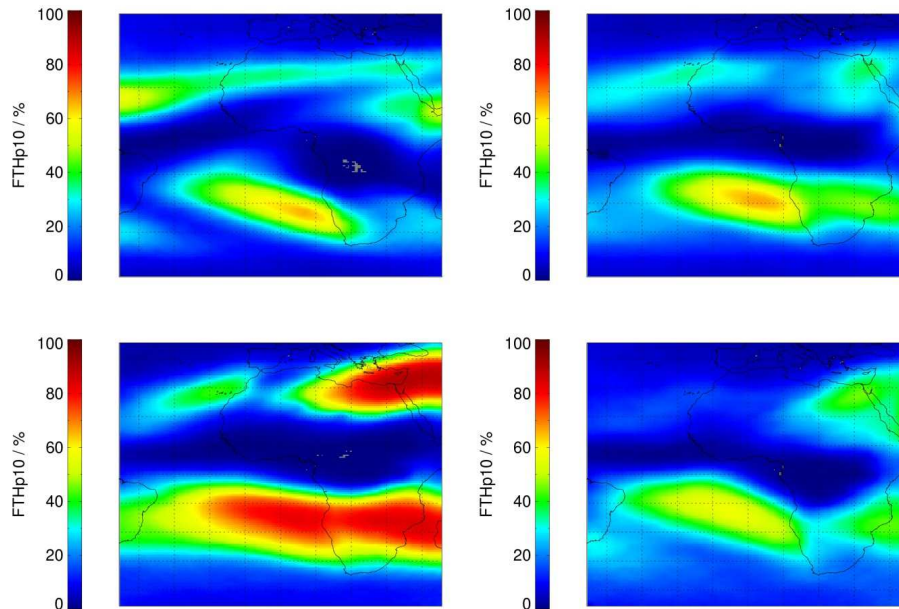
Fig. 7. As Fig. 4 but for the frequency of occurrence of FTH < 10 % (FTHp10). Grey areas: small number of valid observations.
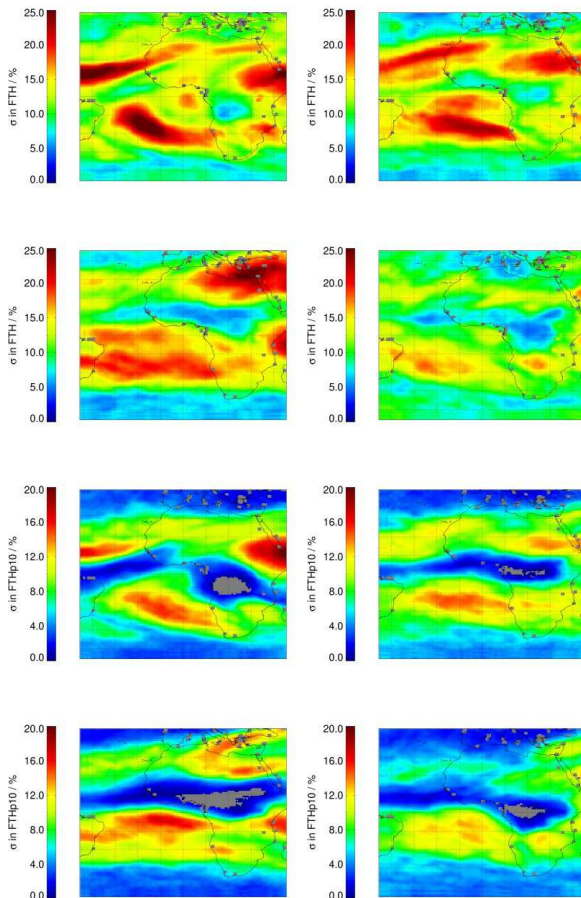
Fig. 8. 1984–2009 relative standard deviation per season in FTH (top four panels) and in FTHp10 (bottom four panels). Order in FTH and FTHp10 panels: DJF, MAM, JJA and SON, clockwise, starting at top left. Areas with small number of valid observations are marked grey.
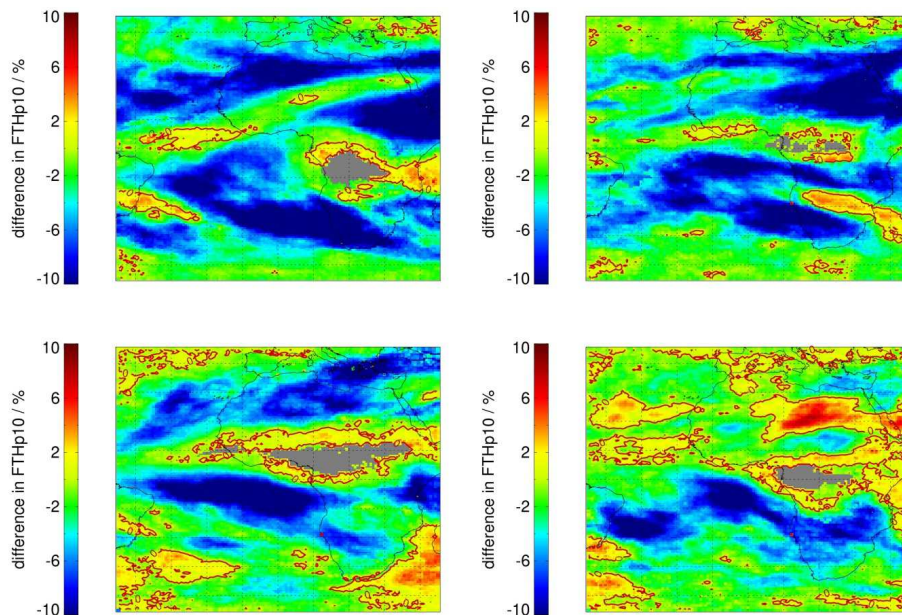
Fig. 9. Difference in decadal averages of FTHp10, computed between 1990–1999 and 2000–2009. The difference was computed per season: DJF (top left panel), MAM (top right panel), JJA (bottom left panel) and SON (bottom right panel). Red contour lines mark 0 % difference. Areas with small number of valid observations are marked grey.
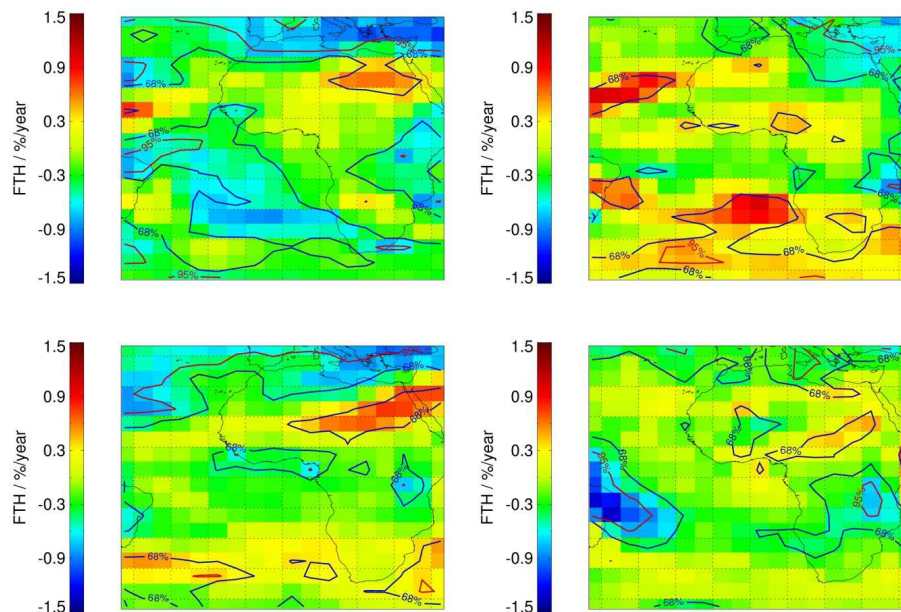
Fig. 10. As Fig. 4 but for the linear trend in relative FTH. The blue and red contour lines mark confidence probabilities of 68 and 95 %, respectively. Areas with small number of valid observations are marked grey.
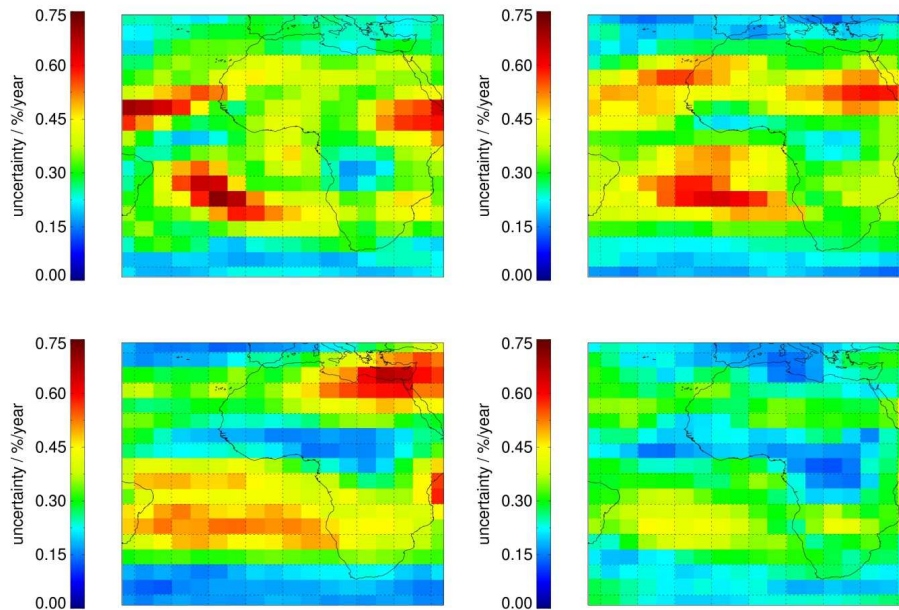
Fig. 11. As Fig. 4 but for the uncertainty of the linear trend in relative FTH.
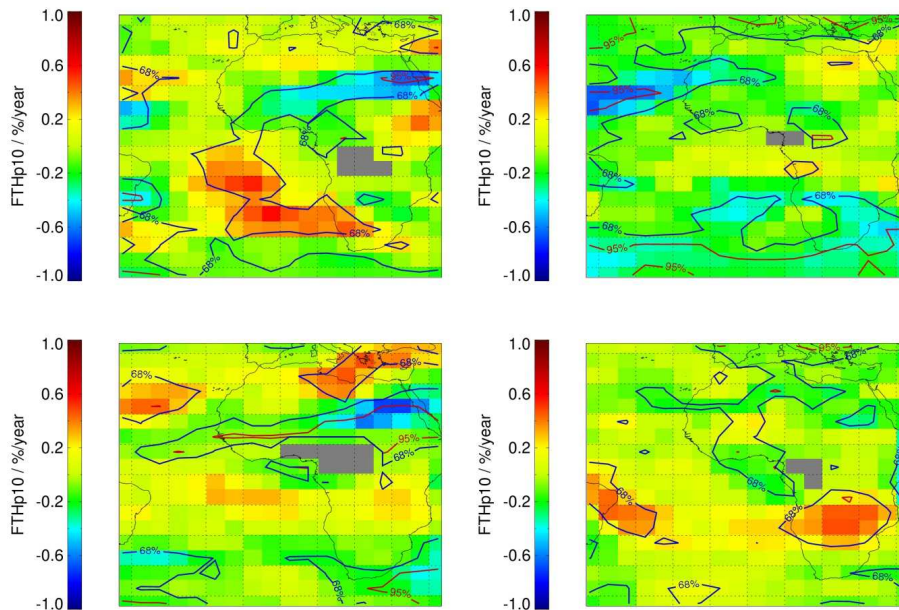
Fig. 12. As Fig. 9 but for FTHp10.

Full Screen / Esc

Printer-friendly Version

Interactive Discussion
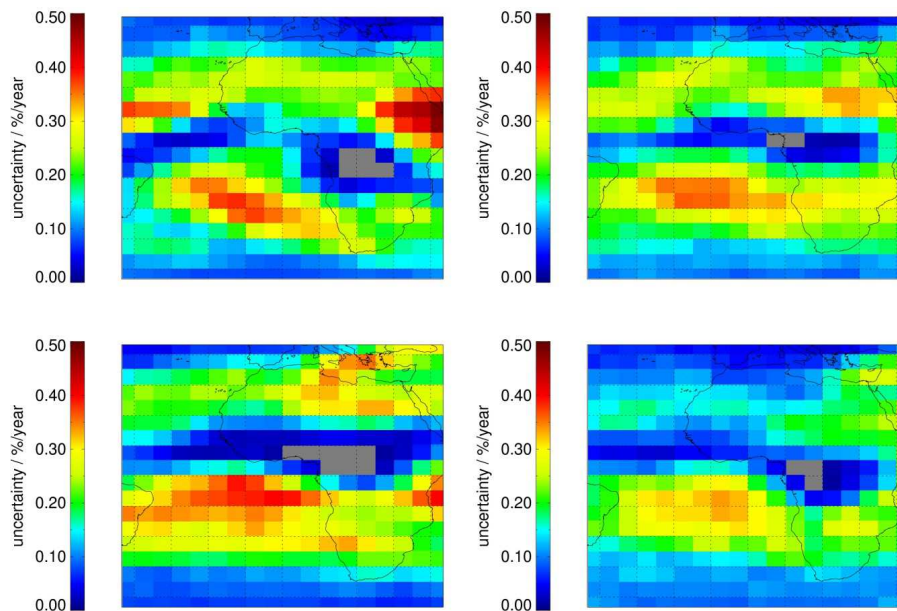
Fig. 13. As Fig. 11 but for the uncertainty of the linear trend in FTHp10.

Full Screen / Esc

Printer-friendly Version

Interactive Discussion